

Phase-field theory of brine entrapment in sea ice: Short-time frozen microstructures

Silke Thoms¹, Bernd Kutschan², Klaus Morawetz^{2,3,4}

¹*Alfred Wegener Institut, Am Handelshafen 12, D-27570 Bremerhaven, Germany*

²*Münster University of Applied Science, Stegerwaldstrasse 39, 48565 Steinfurt, Germany*

³*International Institute of Physics (IIP) Federal University of Rio Grande do Norte Av. Odilon Gomes de Lima 1722, 59078-400 Natal, Brazil and*

⁴*Max-Planck-Institute for the Physics of Complex Systems, 01187 Dresden, Germany*

We analyze the early phase of brine entrapment in sea ice, using a phase field model. This model for a first-order phase transition couples non-conserved order parameter kinetics to salt diffusion. The evolution equations are derived from a Landau-Ginzburg order parameter gradient dynamics together with salinity conservation. The numerical solution of model equations by an exponential time differencing scheme describes the time evolution of phase separation between liquid water with high salinity and the ice phase with low salinity. The numerical solution in one and two dimensions indicates the formation of one dominant wavelength which sets the length scale of short-time frozen structures. A stability analysis provides the phase diagram in terms of two Landau parameters. It is distinguished an uniform ice phase, a homogeneous liquid saline water solution and a phase where solidification structures can be formed. The Landau parameters are extracted from the supercooling and superheating as well as the freezing point temperature of water. With the help of realistic parameters the distribution of brine inclusions is calculated and found in agreement with the measured samples. The size of the ice domains separating regions of concentrated seawater depends on salinity and temperature and corresponds to the size of sea ice platelets obtained from a morphological stability analysis for the solidification of salt water.

PACS numbers: 81.30.Fb, 92.10.Rw, 61.72.Ss

I. INTRODUCTION

The formation of sea ice plays an important role in earth's climate because it determines the large-scale heat and mass transport delivered to the surface of the polar oceans. Dependent on the season, sea ice covers an area of around $(4.3 - 15.7) \times 10^6 \text{ km}^2$ in the Arctic and between $(3.6 - 18.8) \times 10^6 \text{ km}^2$ in the Antarctic [1, 2]. Thus, at its maximum extent, sea ice covers about 10% of the ocean's surface area.

A large number of brine inclusions emerge in sea ice when ice is formed. During the freezing process, solutes in the seawater are excluded from the ice matrix and segregate into brine droplets or in intercrystalline brine layers and at grain boundaries [3, 4]. The size and distribution of brine inclusions depend on the thermal history and growth conditions.

Despite the extreme growth conditions of low temperatures and high salinities, sea ice offers a favorable environment for a variety of organisms, particularly bacteria and microalgae, which live and thrive within the brine inclusions. Brine entrapment in sea ice is a crucial element in the polar ecosystem because it is an important habitat for a variety of CO_2 -binding microalgae. A high lasting biomass yield of $10 - 1000 \text{ mg Chl m}^{-3}$ [5-7] has been measured within sea ice, whereas in the water under the ice chlorophyll is usually below 0.1 mg m^{-3} [6]. Thus, due to the ice-algal growth a concentrated food source is delivered to the low-productivity ice-covered sea. In the months of ice melting, ice algae can provide a starter community for phytoplankton growth by seeding the water column [6]. To unravel the interplay between the

microorganisms and their natural habitat the knowledge of the pore space connectivity and the conditions under which different inclusion morphologies are formed is mandatory.

Understanding the solidification of salt water is a long-standing interest. Already QUINCKE considers ice polluted with any salt as "liquid jelly" with walls and cells [8]. The freezing process of salt water is but one example of the solidification of binary alloys. The thermodynamics and solidification theory of alloys (see e.g. [9, 10]) have been used in a variety of forms to study solidification systems in the context of metallurgical and geological applications. The two-phase region comprising of essentially pure ice crystals bathed in water enriched in the rejected salt is known in the context of binary alloys as a mushy layer. The theory of mushy layers has been applied to explain the bulk features of sea ice. Rather than modelling the small-scale spatial variability, the theory of mushy layers provides predictions of the properties of the mushy layer averaged over the microscale. The equations describing the conservation of mass, heat and salt predict the dynamics of growing sea ice in terms of local mean variables such as temperature and the concentration of the interstitial liquid. Darcy's equation is used to calculate the local mean brine flux in the rigid matrix of ice which is described in terms of the local mean porosity [11, 12].

From a small-scale perspective GOLDEN *et al.* [13-15] discussed the role of percolation transitions in brine trapping during the solidification of seawater. The distribution of brine entrapments and its impact on fluid- and nutrient transport is reported in [15]. As key variable for all transport processes the permeability was intro-

duced. Permeability depends on porosity, as well as on microstructural characteristics of brine inclusions. Porosity, defined as volume fraction of brine inclusions in total ice volume, is a determining feature for biological activity within ice. The microstructure near the ice bottom is particularly important for algae growth. Highest cell abundances occur in this region, due to the higher porosity and to the constant flushing with nutrient-rich seawater [16, 17].

Mushy layers are formed due to a instability of the solidifying interface and are ubiquitous during the solidification of alloys. The theory of morphological stability of sharp interfaces [18, 19] has been used to examine the initial structures formed during the directional solidification of binary alloys. A cellular growth during the solidification is described by CORIELL *et al.* [20]. Growing sea ice at the ocean-atmosphere interface typically consists of an array of small ice platelets with randomly oriented horizontal c-axes which grow vertically downwards from the surface. WETTLAUER [21] applied the morphological stability theory to the solidification of salt water and determined the length scales for ice platelet growth. Phase field methods have improved the early interface stability approaches in terms of the time dependence of length scales and details of crystal shapes involved in pattern formation during directional solidification. However, the more simplistic sharp interface models have been shown to be capable to predict reasonable length scales within crystal growth [22–24]. The influence of natural convection [11] has been shown to be included to properly predict the length scales at the ice-seawater interface [25].

When sea ice grows in turbulent surface water the newly formed platelets of ice are suspended in the water, forming the so-called frazil ice. This first form of new ice agglomerates by the action of wave motion and wind, and by further consolidation it forms larger aggregates such as grease ice and pancake ice. Finally a closed cover of granular ice is developed. This layer is characterized by the loss of prevalent orientation of the ice crystals due to their quick formation under turbulent water conditions. The underside of growing sea ice typically consists of a matrix of pure ice platelets which grow in the direction normal to the interface, forming the so-called skeletal layer. In this regime the platelets are generally parallel and the brine circulates freely in vertical layers parallel to the platelets. Spacings between brine layers are typically 0.1 – 1 mm, depending on the growth rate of the ice [3]. Within the skeletal layer a direct vertical connection to the seawater below exists. As the platelets lengthen and grow wider, small ice bridges form between adjacent platelets, forming the so-called bridging layer. The formation of ice bridges, i. e. trapping inclusions of brine is the source of most of the liquid found in sea ice. Thus, above the skeletal layer, brine tends to be located in vertically oriented sheetlike inclusions.

PRINGLE *et al.* [26] imaged sea ice single crystals with X-ray computed tomography, and found arrays of

near-parallel intracrystalline brine layers whose connectivity and complex morphology varied with temperature. The results of PRINGLE *et al.* [26] clearly show near-parallel layering, but the pore space has been shown to be much more complicated than suggested by simple models of parallel ice lamellae and parallel brine sheets (e.g. [3]). While the morphological instability at the ice-seawater interface is well understood, comparatively little is known, however, about the inclusions of brine due to the formation of ice bridges between the growing ice platelets. Several interface stability approaches provided details of ice platelet shapes, but they do not address pattern formation during the freezing of the liquid sandwiched between ice platelet boundaries. In a step towards the development of a predictive model of sea ice microstructure, we develop a phase field model for the pattern formation during solidification of the two-dimensional interstitial liquid. We use the model to calculate the short-time frozen microstructures and compare our findings with the vertical brine pore space obtained from X-ray computed tomography [26].

In former work we have used the Turing mechanism to describe brine entrapment in sea ice without salinity conservation [27]. In this paper we develop a theory that includes both macroscopic salt diffusion and microscopic order parameter dynamics. In such a so-called phase field model the two variables (salinity and order parameter) are coupled in two ways: salt is rejected from freezing water and accumulates in the water adjacent to the growing ice, and as the rejected salt causes the salinity of the seawater to increase, the free energy that determines the order parameter dynamics is modified. In this paper we examine two phase field equations which describe the time evolution of the non-conserved, Landau-Ginzburg order parameter coupled to a spatially varying conserved field. Choosing the total mass of salt as the conserved variable as done by GRANDI [28] it follows a model in which the order parameter is coupled to the local salinity. In fact, the author also developed a phase field approach for the solidification and solute separation in water solutions. Both phase field approaches differ in the choice of the free energy functional. GRANDI [28] started from a free energy functional which is able to reproduce the equilibrium conditions for the coexistence of ice and solute at critical concentration. We describe the free energy according to the classical Landau-Ginzburg theory of a first-order phase transition, i. e. in terms of a power series expansion of the free energy in the order parameter. The Landau coefficient functions we extract from the thermodynamic properties of pure water in a way such that the equilibrium as well as the metastable states of the ice/water system is well defined. One important difference is that GRANDI [28] calculated the equilibrium phase profiles in one dimension, whereas we consider the short-time frozen structures, which are non-equilibrium phases. Here we develop a micrometer scale model where we neglect the spatial temperature gradient in ice or water. Solving our phase field equations in one and two spatial dimensions

we find that short-time frozen structures appear which are in a good agreement with the observed patterns.

The outline of the paper is as follows. In the next chapter we derive the model equations from a variational principle. The linear stability analysis is presented in the second chapter leading to the parameter range where structure can be formed. The numerical solution and the comparison with the experimental data complete the fourth section. In the fifth section we summarize and conclude.

II. MODEL DEVELOPMENT

A. Structure properties and order parameter of water and ice

We restrict to a hexagonal ice-I modification, the so-called I_h , and search for a variable u which minimizes the free energy \mathfrak{F} . This variable u should describe the orderliness of water molecules as it was introduced by MEDVEDEV *et al.* [29]. Ideal pure hexagonal ice possesses an exact tetrahedral structure (see Fig. 1 below). Therefore the measure of the state of order is the "tetrahedrality"

$$u \sim 1 - M_T = 1 - \frac{1}{15 \langle l^2 \rangle} \sum_{i,j} (l_i - l_j)^2, \quad (1)$$

where l_i are the lengths of the six edges of the tetrahedron formed by the four nearest neighbors of the considered water molecule. For an ideal tetrahedron one has $M_T = 0$ and the random structure yields $M_T = 1$.

In this way it is possible to discriminate between ice- and water molecules via a two-state function. This corresponds to the idea of WILHELM CONRAD RÖNTGEN, who distinguished between molecules of the first kind, which he called ice molecules and molecules of the second kind [30] representing the liquid aggregate state.

The equations of the model we derive from non-conserved, Landau-Ginzburg order parameter kinetics together with salinity conservation assuming the total free energy in d-dimensions

$$\mathfrak{F} = \int \left\{ \frac{1}{2} K [\nabla u(x, t)]^2 + f[u(x, t), v(x, t)] \right\} d^d x \quad (2)$$

with the energy density for the order parameter u and the salinity v

$$f(u, v) = \frac{a'_1}{2} u^2 - \frac{a_2}{3} u^3 + \frac{a_3}{4} u^4 + \frac{h}{2} u^2 v + \frac{b_1}{2} v^2 - b_0 v. \quad (3)$$

The parameter a'_1 is the temperature-dependent freezing parameter determining the phase transition. The temperature dependence of the cubic and quartic terms of the Landau-Ginzburg-functional (2) is supposed to be so weak near the phase transition that they can be well approximated as positive constants, namely, a_2 and a_3 .

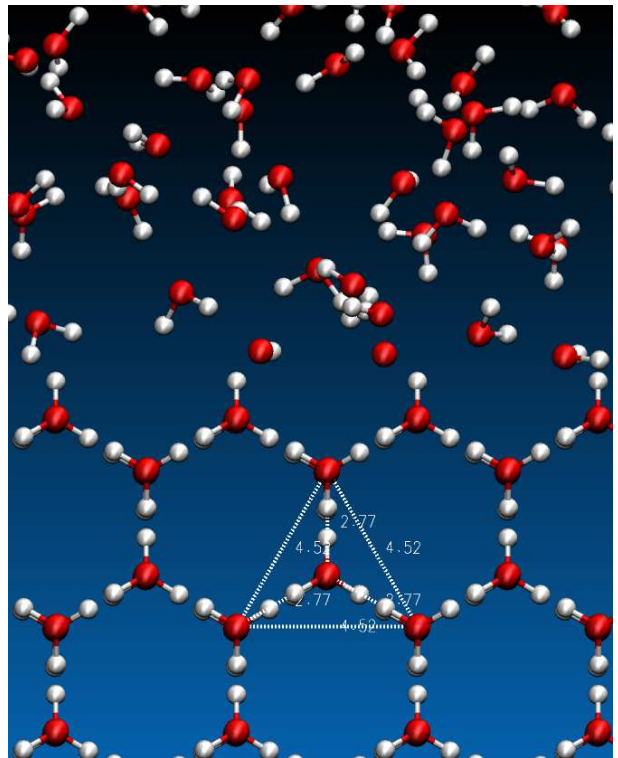


FIG. 1: Change from a regular hexagonal lattice structure to irregular bonds during the melting of ice: water at 300K (above) and hexagonal ice (below).

The structure parameter a_3 is responsible for the stability of the ordered phase, K is the gradient energy coefficient of order parameter fluctuations, and b_1 determines the salinity fluctuations. The coefficient a_2 is connected with an uneven exponent and is therefore responsible for possible phase transitions of first kind. The coefficient h describes the interaction between the order parameter u and the salinity v . We will see soon that these parameters can be scaled to only three relevant parameters where the phase diagram is determined only by two of them, the dimensionless structure and freezing parameter.

The variation of the Landau-Ginzburg free energy (2) yields the gradient dynamics for the order parameter u

$$\frac{\partial u}{\partial t} = -\Gamma \frac{\delta \mathfrak{F}}{\delta u} = \Gamma (-a'_1 u + a_2 u^2 - a_3 u^3 - h u v + K \Delta u), \quad (4)$$

where Γ is a relaxation coefficient for u which determines the time scale of the ordering process. Further we want to assume that the total mass of salt is conserved. Therefore we demand to have a balance equation of the form $\partial v / \partial t = -\nabla \cdot \vec{j}$ where the current is assumed to be proportional to a generalized force $\vec{j} = M \vec{f}$ which should be given by a potential as $\vec{f} = -\nabla P$. This potential in turn is given by the variation of the free energy density $P = \delta \mathfrak{F} / \delta v$. This procedure is nothing but the second law of Fick. With the assumption that salt is a

passive tracer which does not undergo a phase transition, we obtain an equation of Cahn-Hilliard-type without the fourth derivation for the evolution of the salinity v

$$\frac{\partial v}{\partial t} = \nabla \left(M \nabla \frac{\delta \mathcal{F}}{\delta v} \right) = M \left(\frac{h}{2} \Delta u^2 + b_1 \Delta v \right). \quad (5)$$

The coefficient M is the mobility, which is considered as constant. This linearisation of the equation is valid for the early phase of brine entrapment where the brine pore space is connected.

Defining the reduced time and spatial coordinates

$$\tau = \frac{\Gamma b_1 a_2^2}{h^2} t, \quad \xi = \sqrt{\frac{\Gamma}{M}} \frac{a_2}{h} x \quad (6)$$

as well as dimensionless order parameters of ice/water structure and salinity

$$\psi = \frac{h^2}{b_1 a_2} u, \quad \rho = \frac{h^3}{b_1 a_2^2} v \quad (7)$$

the model equations (4) and (5) can be written in reduced form

$$\frac{\partial \psi}{\partial \tau} = -\alpha'_1 \psi + \psi^2 - \alpha_3 \psi^3 - \psi \rho + D \frac{\partial^2 \psi}{\partial \xi^2} \quad (8)$$

$$\frac{\partial \rho}{\partial \tau} = \frac{1}{2} \frac{\partial^2 \psi^2}{\partial \xi^2} + \frac{\partial^2 \rho}{\partial \xi^2}. \quad (9)$$

The benefit of this form is that the dynamics of the dimensionless order parameter ψ and the dimensionless salinity ρ depends only on three parameters, the freezing parameter

$$\alpha'_1 = \frac{a'_1 h^2}{a_2^2 b_1}, \quad (10)$$

the structure parameter

$$\alpha_3 = \frac{a_3 b_1}{h^2}, \quad (11)$$

and the diffusivity $D = \frac{D_{\text{ice}}}{D_{\text{salt}}}$ with $\alpha_1, \alpha_3, D > 0$. The diffusivity $D_{\text{ice}} = \Gamma K$ describes the propagation of the order parameter, and $D_{\text{salt}} = M b_1$ the diffusion of salt. The parameters α'_1 and α_3 define the regions for the ordered and non-ordered phase. Their physical meaning will be more transparent when the results are discussed in terms of thermodynamic properties of water.

III. LINEAR STABILITY ANALYSIS

A. Uniform stationary solution

The following linear stability analysis is related to one spatial dimension. The extension to higher dimensions is straight forward.

In terms of the reduced quantities, the free energy density (3) for a uniform order parameter and salinity

$$\psi = \psi_0 = \text{const}, \quad \rho = \rho_0 = \text{const} \quad (12)$$

takes the form

$$f(\Psi_0, \rho_0) = \alpha_0 + \frac{\alpha_1}{2} \psi_0^2 - \frac{1}{3} \psi_0^3 + \frac{\alpha_3}{4} \psi_0^4 \quad (13)$$

where α_1 and α_0 depend on the salinity ρ_0 as

$$\begin{aligned} \alpha_0 &= \frac{1}{2} \rho_0^2 - \gamma \rho_0 \\ \alpha_1 &= \alpha'_1 + \rho_0. \end{aligned} \quad (14)$$

Important for the further description of seaice formation is the compound parameter α_1 . The sum (14) includes both the temperature-dependent parameter α'_1 and the salinity ρ_0 . If the parameter α'_1 corresponds to a certain freezing point temperature then $\alpha'_1 + \rho_0$ corresponds to a lower transition temperature. This effect is known as freezing-point depression.

Note that α_0 is the value of f in the disordered phase, which is characterized by $\psi_0 = 0$. Since α_0 is a constant background term, which is merely dependent on the total salinity, it can be taken to be zero for the subsequent discussion, i.e.

$$f(\Psi_0, \rho_0) = \psi_0^2 \left(\frac{\alpha_1}{2} - \frac{1}{3} \psi_0 + \frac{\alpha_3}{4} \psi_0^2 \right). \quad (15)$$

The function f versus the dimensionless order parameter for various α_1 is shown in Fig. 2(a). The locations of the extrema of f are given by the stationary condition

$$\frac{\partial f}{\partial \psi_0} = 0 = \psi_0 (\alpha_1 - \psi_0 + \alpha_3 \psi_0^2) \quad (16)$$

whose solutions have a minimum (assuming $\alpha_1 > 0$)

$$\psi_0^0 = 0 \quad (17)$$

and a minimum/maximum for

$$\psi_0^\pm = \frac{1}{2\alpha_3} (1 \pm \sqrt{1 - 4\alpha_1\alpha_3}). \quad (18)$$

At sufficient high $\alpha_1 > 1/4\alpha_3$, the minimum at $\psi_0^0 = 0$ is the only allowed physical solution, which is the disordered state. As soon as

$$\alpha_1 \leq \frac{1}{4\alpha_3} \quad (19)$$

a second relative minimum appears at ψ_0^+ . Which of these minima establishes the state of lowest free energy is dependent on the critical $\alpha_{1,c}$ which is found from the coexistence curve where these two local minima are equal and $f(\Psi_0^+) = f(\Psi_0^0) = 0$ which yields

$$\alpha_{1,c} = \frac{2}{9\alpha_3}. \quad (20)$$

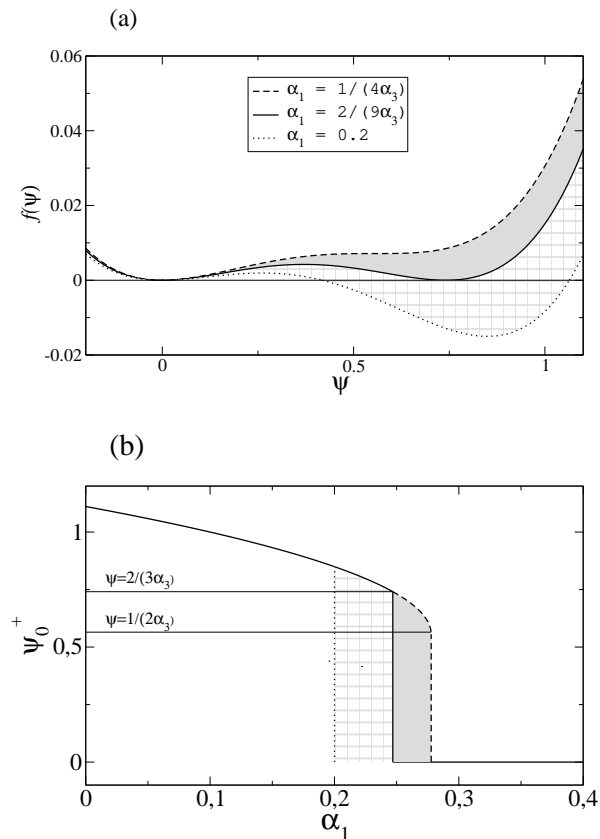


FIG. 2: Condition for a first-order phase transition. (a) The free energy density f versus the uniform dimensionless order parameter (tetrahedricty) for various freezing parameter α_1 and the structure parameter $\alpha_3 = 0.9$. (b) Dependence of absolute minimum of the free energy density (18) on α_1 (solid line). The dashed line corresponds to the position of the second minimum and the dotted line indicates if one jumps from the first minimum to the absolute one in figure (a). In the checked-pattern region a first-order phase transition can occur and the ordered phase ψ_0^+ is stable. In the gray region, the ordered phase ψ_0^+ is metastable whereas the non-ordered phase ψ_0 is stable.

The coexistence curve is plotted as solid line in Fig. 2(a) and its second minima becomes $\psi_0^+(\alpha_{1,c}) = \frac{2}{3\alpha_3}$. Above the critical parameter $\alpha_{1,c} < \alpha_1 < \frac{1}{4\alpha_3}$ the ordered phase $\psi_0^+ > 0$ is metastable whereas the non-ordered phase ($\psi_0 = 0$) is stable. This is illustrated as gray area in Fig. 2(a). As soon as α_1 decreases approaching $\alpha_1 = \alpha_{1,c}$ the second minimum at $\psi_0^+ > 0$ becomes deeper than the minimum at $\psi_0 = 0$ and the ordered phase ψ_0^+ becomes stable. This is illustrated as checked pattern area. Therefore the absolute minimum is dependent on a discontinuous change of the order parameter from $\psi_0 = 0$ to $\psi_0^+ > 0$ as plotted in Fig. 2(b).

B. Conditions for structure formation

The fixed points for the kinetics (8) and (9) are given by the local extrema of the Landau function f as discussed in the foregoing paragraph. In order to derive the conditions for structure formation, we perform a linear stability analysis for the two local minima around the disordered phase ψ_0^0 and the ordered phase ψ_0^+ by linearizing the equation system (8) and (9) according to $\psi = \psi_0 + \bar{\psi}$ and $\rho = \rho_0 + \bar{\rho}$. For the time evolution of the linear perturbations $\bar{\psi}$ and $\bar{\rho}$ one gets the equation system

$$\begin{pmatrix} \frac{\partial \bar{\psi}}{\partial \tau} \\ \frac{\partial \bar{\rho}}{\partial \tau} \end{pmatrix} = \begin{pmatrix} \aleph + D \frac{\partial^2}{\partial \xi^2} & -\psi_0 \\ \psi_0 \frac{\partial^2}{\partial \xi^2} & \frac{\partial^2}{\partial \xi^2} \end{pmatrix} \begin{pmatrix} \bar{\psi} \\ \bar{\rho} \end{pmatrix}. \quad (21)$$

Here $\aleph = -\alpha_1 + 2\Psi_0 - 3\alpha_3\Psi_0^2$ which takes the value $\aleph = -\alpha_1$ for the fixed point $\Psi_0^0 = 0$ and $\aleph = \psi_0 - 2\alpha_3\psi_0^2$ for Ψ_0^+ .

As commonly used, the Fourier ansatz $\bar{\rho} = \rho_0 \exp[\lambda(\kappa)\tau + i\kappa\xi]$ and analogously for $\bar{\psi}$ results into the characteristic equation for the growth rate $\lambda(\kappa)$

$$\lambda(\kappa)^2 + [(D+1)\kappa^2 - \aleph] \lambda(\kappa) + q(\kappa^2) = 0 \quad (22)$$

with

$$q(\kappa^2) = \kappa^2 [D\kappa^2 - \aleph - \psi_0^2]. \quad (23)$$

The two possible growth rates read

$$\lambda_{1,2} = -\frac{1}{2} [(D+1)\kappa^2 - \aleph \pm \sqrt{\Delta}] \quad (24)$$

with

$$\begin{aligned} \Delta &= [(D+1)\kappa^2 - \aleph]^2 - 4q(\kappa^2) \\ &= [(D-1)\kappa^2 - \aleph]^2 + 4\kappa^2\psi_0^2 > 0. \end{aligned} \quad (25)$$

Time-oscillating structures can appear only if $\text{Im } \lambda(\kappa) \neq 0$, i.e. $\Delta < 0$, which can never be fulfilled since (25) can be expressed as a sum of two real squared numbers. In other words we do not have time-growing oscillating structures in our model.

The condition for structure formation is the instability of the fixed point, where some spatial fluctuations may be amplified and form macroscopic structures. An unstable fixed point which is associated with positive eigenvalues $\lambda(\kappa) > 0$ allows any fluctuation with a wave-vector κ to grow exponentially in time. Therefore, we search for eigenvalues which possess a positive real part for a positive wave number, i.e. $\text{Re } \lambda(\kappa) > 0$ and $\kappa^2 > 0$.

The condition for structure formation is not satisfied for each fixed point. For the fixed point representing the disordered phase, $\psi_0 = 0$ and $\rho_0 = \text{const}$, one sees from (24) that there are no positive real eigenvalues

$$\lambda_{1,2} = \frac{1}{2} [-(D+1)\kappa^2 - \alpha_1 \pm |(D-1)\kappa^2 + \alpha_1|] < 0 \quad (26)$$

see also Fig. 3. Consequently, there is no structure formation in this state which was expected for the disordered phase, of course.

Now lets concentrate on the fixed point for the ordered phase Ψ_0^+ of (18). There are two distinct roots (24), both of which are real numbers. For the condition of time-growing fluctuations we search now for the condition $\lambda(\kappa) > 0$. The coefficient of the linear term of equation (22) is positive since $-\aleph = 2\alpha_3\psi_0^2 - \psi_0 > 0$ for $\psi_0 = \psi_0^+ > 1/(2\alpha_3)$ and κ^2 as well as $D > 0$. Therefore, the first term in (24) is negative and we can only have a positive $\lambda(\kappa) > 0$ if the square of this term is less than the discriminant Δ . This leads to the condition $q(\kappa^2) < 0$. The latter is illustrated for the parameters $\alpha_3 = 0.9$, $\alpha_1 = 0.2$, and $D = 0.5$ in Fig. 3, which shows $\lambda(\kappa)$ versus the dimensionless wave number κ along with $q(\kappa^2)$.

We can only have positive $\lambda(\kappa)$ if the values of κ are restricted to the region between the zeros of $\lambda(\kappa)$, which coincide with the roots of the equation

$$q(\kappa^2) = [-\psi_0 + (2\alpha_3 - 1)\psi_0^2 + D\kappa^2]\kappa^2 = 0. \quad (27)$$

Hence, the κ region is restricted to the interval

$$\kappa^2 \in \left(0, \frac{\psi_0}{D} [1 - (2\alpha_3 - 1)\psi_0]\right) \quad (28)$$

with $\psi_0 = \psi_0^+$. The upper boundary of the interval must be positive, and we get only a meaningful condition from (28) if $\psi_0 [1 - (2\alpha_3 - 1)\psi_0]/D > 0$. Discussing separately the cases $\alpha_3 \geq 1/2$ one sees that (28) gives no additional restriction on α_1 and D for $\alpha_3 \leq 1/2$. For the case $\alpha_3 > 1/2$ we get the restriction

$$(2\alpha_3 - 1)\sqrt{1 - 4\alpha_1\alpha_3} < 1, \quad \alpha_1 > 0, \quad \alpha_3 > 0. \quad (29)$$

Moreover, the latter one has to be in agreement with the condition for the occurrence of a first-order phase transition (20)

$$0 < \alpha_3 < \frac{2}{9\alpha_1}. \quad (30)$$

Solving the set of inequalities given by (29) and (30), we obtain the range for structure formation

$$\begin{aligned} 2 > \alpha_3 > 1: & \quad \frac{1}{4\alpha_3} \left(1 - \frac{1}{(2\alpha_3 - 1)^2}\right) < \alpha_1 < \frac{2}{9\alpha_3} \\ 1 > \alpha_3 > 0: & \quad 0 < \alpha_1 < \frac{2}{9\alpha_3} \end{aligned} \quad (31)$$

In Fig. 4 we present this in form of a phase diagram for the freezing and structure parameters. One can see that the instability region starts at the maximal point $\alpha_1 = 1/9$ at $\alpha_3 = 2$ which means that we have only a structure formation for sufficiently small structure parameters $\alpha_3 < 2$ and proper bound on the freezing parameter α_1 , see (31).

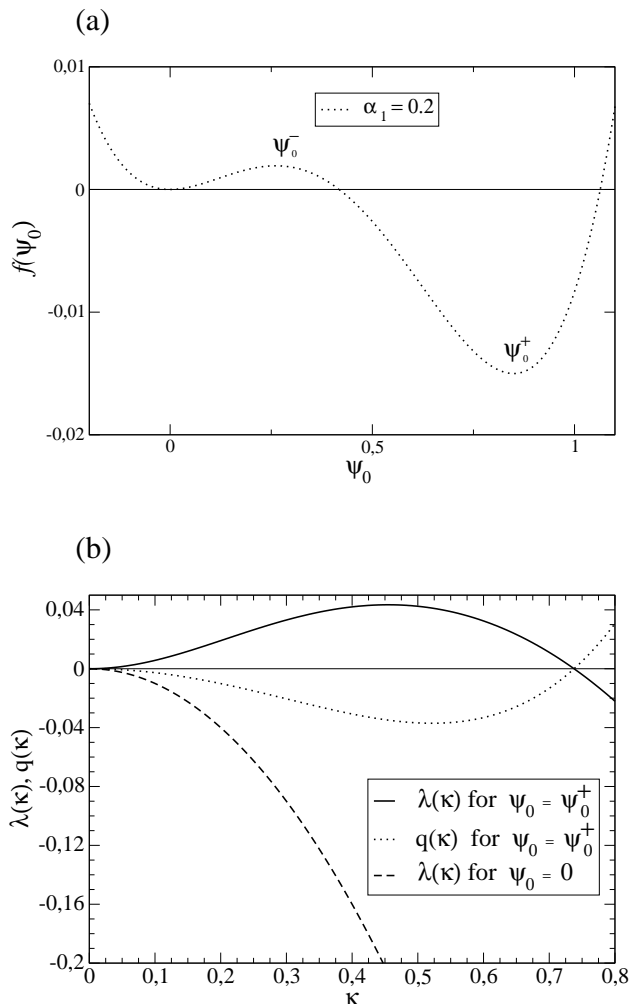


FIG. 3: Conditions for structure formation. (a) The free energy density f versus the uniform dimensionless order parameter for $\alpha_1 < \alpha_{1,c}$. (b) Eigenvalues $\lambda(\kappa)$ versus the dimensionless wave number κ for $\alpha_3 = 0.9$, $\alpha_1 = 0.2$, and $D = 0.5$ along with the function $q(\kappa^2)$ of equation (23).

The description of the instability region does not involve a restriction on the diffusivities of salt and water. This is different from the model of KUTSCHAN *et al.* [27], which describes structure formation in seaice in terms of Turing structures. The latter can only exist if the difference between the diffusion coefficients of salt and water is sufficiently large. In the present study, the diffusivity D enters the range for the possible wave numbers of unstable modes only. According to (28) it is given explicitly by

$$\kappa^2 \in \left[0, \frac{\alpha_1}{D} \left(2 - \frac{1}{\alpha_3}\right) + \frac{(1 - \alpha_3)(1 + \sqrt{1 - 4\alpha_1\alpha_3})}{2D\alpha_3^2}\right]. \quad (32)$$

Fig. 4 shows the influence of the structure parameter α_1 on the formation of a solidification microstructure. A

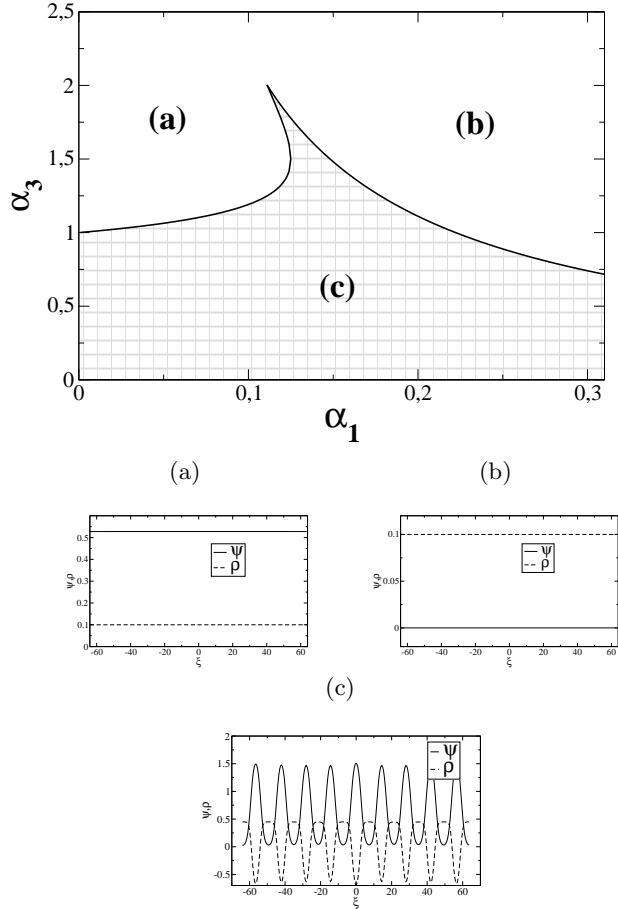


FIG. 4: The instability region of the fixed point ψ_0^+ of (18) and $\rho_0 = \text{const}$ as phase diagram together with selected structures: (a) $\alpha'_1 = 0.01$, $\rho(\tau = 0) = 0.1$, $\alpha_3 = 1.5$, (b) $\alpha'_1 = 0.2$, $\rho(\tau = 0) = 0.1$, $\alpha_3 = 0.9$, (c) $\alpha'_1 = 0.1$, $\rho(\tau = 0) = 0.1$, $\alpha_3 = 0.9$. In the checked region spatial structures can occur.

small α_1 means low temperatures and/or low salinities and consequently a freezing process. Therefore we find in the region (a) the uniform ice phase and a inclusion of salt as a function of the structure parameter α_3 . In contrast in the region (b) there are higher temperatures and/or higher salinities. This induces a melting with a uniform liquid water phase and dissolved salt. Finally the spatial structures can appear in region (c).

C. Mechanism of phase separation

The formation of a spatial structure is driven by the instability of the uniform stationary solution $\psi_0 = \psi_0^+$ and $\rho_0 = \text{const}$, as discussed in the previous chapter. The instability becomes evident in terms of a positive eigenvalue $\lambda(\kappa)$ for a range of wave numbers κ as seen in Fig. 3. Hence, any linear perturbation with a wave

number κ inside the region between the zeros of $\lambda(\kappa)$ grows exponentially with amplification factor $\lambda(\kappa)$. The function $\lambda(\kappa)$ has a maximum at a critical wave number κ_c , which defines the fastest-growing wave-vector

$$\kappa_c^2 = \frac{\psi_0}{(D-1)^2} \left[(D-1)(1-2\alpha_3\psi_0) - 2\psi_0 + \frac{(D+1)\psi_0^{1/2}\sqrt{(D-1)(2\alpha_3\psi_0-1)+\psi_0}}{\sqrt{D}} \right] \quad (33)$$

with $\psi_0 = \psi_0^+$ of (18). The expression for κ_c can be approximated by the location of the minimum of the function $q(\kappa^2)$ in equation (23)

$$\kappa_c^2 \approx \frac{(1-2\alpha_3)\psi_0^2 + \psi_0}{2D}. \quad (34)$$

The critical wave number sets the length scale on which phase separation occurs. The size of the initial structure can be estimated by $2\pi/\kappa_c$. The size of the structure depends on the parameters α_1 , α_3 , and D as seen in (33) or (34). With the parameters chosen in Fig. 3, we obtain a pattern size of 13.81. Let us note already here that we have chosen these parameters according to the physical properties of water as will be considered in chapter IV.

D. Numerical solution

In order to proof the relevance of the linear stability analysis of the chapters above and to calculate the time evolution of phase separation, we now solve the equation system (8) and (9) numerically in one and two space dimensions. For this purpose we use the so-called exponential time differencing scheme of second order (ETD2) [31] with the help of which a stiff differential equation of the type $\dot{y} = ry + z(y, t)$ with a linear term ry and a nonlinear part $z(y, t)$ can be solved. The linear equation is solved formally and the integral over the nonlinear part is approximated by a proper finite differencing scheme.

For the one-dimensional case, we plot snapshots of the time evolution of the order parameter ψ and the salinity ρ in Fig. 5. The evolution of the order parameter ψ and the salinity ρ in two dimensions is shown in Fig. 6. The quantities ψ and ρ are opposite in phase to each other. Regions of high salinity correspond to the water phase and regions of low salinity to ice domains. During the freezing process we observe a desalinization of ice and an increase of the salinity in the liquid phase. In the numerical solution a small initial random perturbation is applied to the salinity $\rho(\tau = 0)$ normally distributed having zero mean and variance one. In Fig. 5 we see that one single mode develops given by the wave number κ_c . Similar to the one-dimensional case, we see the formation of one dominant wavelength also in two dimensions (Fig. 6). In the next chapter, we compare the model result for the pattern size to the experimental quantities.

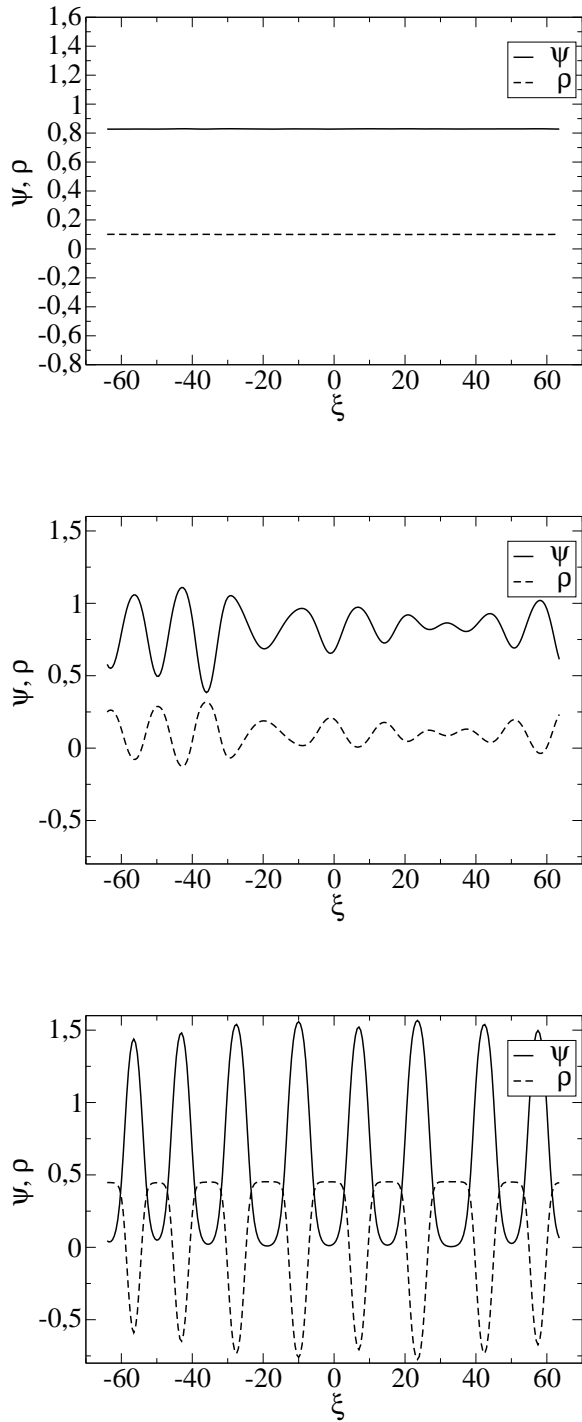


FIG. 5: Time evolution of the order parameter ψ and salinity ρ versus spatial coordinates for $\tau = 10, 150, 500$ (from above to below) for $\alpha_3 = 0.9$, $\alpha'_1 = 0.1$, and $D = 0.5$ with the initial conditions $\psi(\tau = 0) = 0.9$ and a randomly distributed $\rho(\tau = 0) = 0.1 \pm 0.001$.

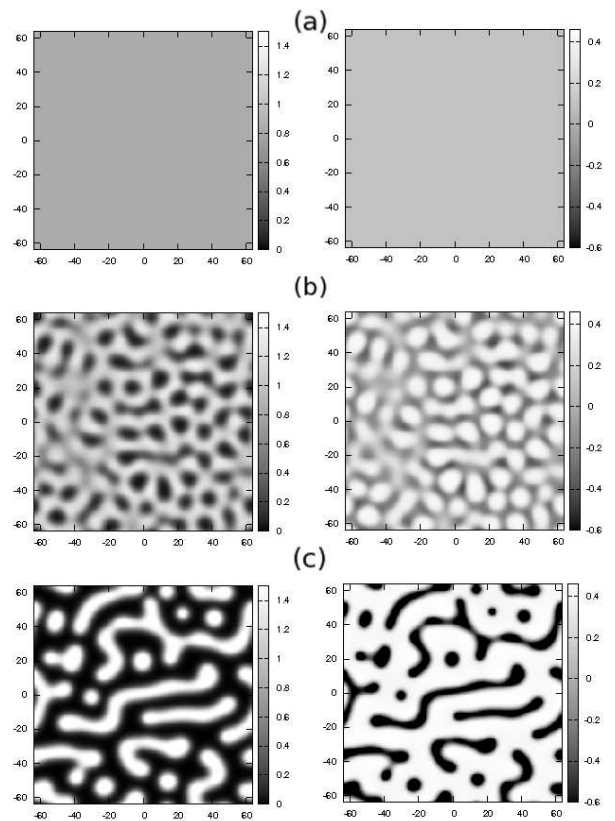


FIG. 6: Time evolution of the order parameter ψ (left) and salinity ρ (right) versus spatial coordinates for $\tau = 10, 150, 500$ (from above to below) with the initial random distribution $\psi(\tau = 0) = 0.9$ and $\rho(\tau = 0) = 0.1 \pm 0.001N(0, 1)$. The parameters are $\alpha_3 = 0.9$, $\alpha'_1 = 0.1$, and $D = 0.5$.

IV. COMPARISON WITH THE EXPERIMENT

A. Determination of parameters from water properties

1. Temperature-dependent representation

The thermodynamic function of state selected for the phase field simulation depends on the definition of the problem. Entropy is appropriate for a system of constant energy and volume, the Helmholtz free energy is the proper choice for an isothermal system at constant volume, and the Gibbs free energy when the temperature and pressure are kept constant. The phase field equations of our study are in terms of the Landau-Ginzburg free energy functional (2). The Landau-Ginzburg free energy functional can be thought of as a Helmholtz free energy or as a Gibbs free energy. We consider the Gibbs free energy as the short-time structures are usually formed under constant pressure, and the experimental data of water properties are based on isothermal-isobar conditions. Now we are going to discuss the two crucial pa-

parameter α_1 and α_3 in terms of their temperature dependence. In this way we will be able to extract the physical meaning of the different instability regions and link the chosen values of the parameters to the supercooling and superheating as well as freezing point temperature of water. The idea consists in identifying the upper borderline of stable structure formation (20) with the freezing point temperature since this is the line where structure, i.e. ice formation is possible at all. In the same manner we identify the borderline of metastable structure (19) with the superheating temperature.

The freezing point temperature depends on the salinity. The solidification of seawater is approximated as that of a dilute aqueous NaCl solution, since Na^+ and Cl^- are the dominant ions in seawater. Hence, the mean salinity in seawater of 35 g/kg corresponds to 1 NaCl molecule per 100 H_2O -molecules, i.e. 1 Na^+ and 1 Cl^- per 100 H_2O -molecules in solution after the dissociation or a ratio of $x = (n_{\text{Na}^+} + n_{\text{Cl}^-})/n_{\text{H}_2\text{O}} = 1/50$. Using the Clausius-Clapeyron (cc) relation

$$\Delta T_{cc} = -\frac{xRT^2}{\Delta H}, \quad (35)$$

where $\Delta H = 6 \frac{\text{kJ}}{\text{mol}}$ is the latent heat of the phase transition from water to ice, $R=8.314 \frac{\text{J}}{\text{molK}}$ is the universal gas constant and $T=273 \text{ K}$, we obtain a freezing point depression from 0°C to -2°C in agreement with the natural value of $\Delta T = -1.9 \text{ K}$. The temperature and salinity dependence of the phase transition is described by the coefficient of the quadratic term in ψ of the Landau-Ginzburg functional

$$\alpha_1(T) = \alpha'_1(T) + \rho_0. \quad (36)$$

Because of the requirement that $\alpha'_1(T_c^0) = 0$ at the lower limit of the supercooling region of fresh water, $T_c^0 = 233.15 \text{ K}$ ([32, 33]), the parameter $\alpha'_1(T)$ is approximated by

$$\alpha'_1(T) = \tilde{\alpha}_1(T - T_c^0), \quad (37)$$

where $\tilde{\alpha}_1$ is a temperature-independent coefficient. The temperature and salinity dependence of the quartic term of the dimensionless Landau-Ginzburg functional is supposed to be so weak near the phase transition that it can be well approximated as a positive constant, namely, α_3 . Using the equations (36), (37) and (10), we obtain for the freezing point depression in the framework of the Landau-Ginzburg theory the expression

$$\Delta T = -\frac{\rho_0}{\tilde{\alpha}_1} = -\frac{b_1 a_2^2}{\tilde{\alpha}_1 h^2} \rho_0. \quad (38)$$

Introducing the salinity-dependent supercooling temperature

$$T_{c,s}^0 = T_c^0 - |\Delta T| \quad (39)$$

the freezing parameter α_1 depends on the temperature according to

$$\alpha_1(T) = \rho_0 \frac{T - T_{c,s}^0}{|\Delta T|}. \quad (40)$$

Besides the supercooling temperature we have two further specific values of the freezing parameter α_1 corresponding to two additional temperatures

$$\alpha_1(T_1) = \rho_0 \frac{T_1 - T_{c,s}^0}{|\Delta T|} = \frac{1}{4\alpha_3} \quad (41)$$

$$\alpha_1(T_c) = \rho_0 \frac{T_c - T_{c,s}^0}{|\Delta T|} = \frac{2}{9\alpha_3} \quad (42)$$

defining the temperatures T_1 and T_c . The shaded area in Fig. 7 describes the supercooling region between T_c and $T_{c,s}^0$. Above this area we find the superheating region for $T_c < T < T_1$.

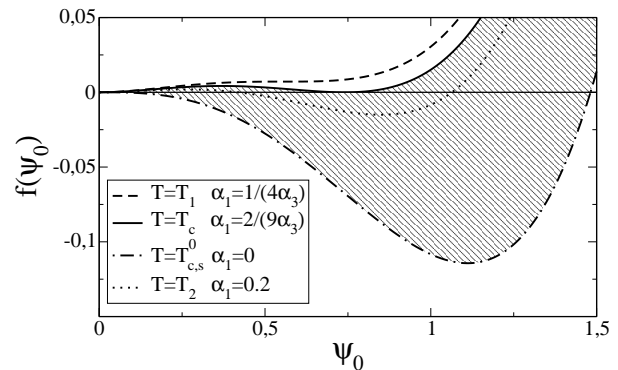


FIG. 7: Representation of supercooling region for freezing of hexagonal ice $T_{c,s}^0 < T_c$ (shaded area) and the superheating region $T_c < T < T_1$.

For the relative minimum for the order parameter ψ_0^+ in (18) we obtain with respect to (40) and (42) the temperature dependence

$$\psi_0^+(T) = \frac{3}{4} \psi_{0,c} \left(1 + \sqrt{1 - \frac{8}{9} \frac{T - T_{c,s}^0}{T_c - T_{c,s}^0}} \right). \quad (43)$$

where the position $\psi_{0,c} = \psi_0(T = T_c) = \frac{2}{3\alpha_3}$ of the coexistence line corresponds to the freezing point temperature T_c . Analogously to Fig. 2 we plot in Fig. 8 the relative minimum ψ_0^+ of the free energy but now versus temperature.

Alternatively we can express the fixed point by the superheating temperature (41) as well since

$$4\alpha_1(T)\alpha_3 = \frac{8}{9} \frac{T - T_{c,s}^0}{T_c - T_{c,s}^0} = \frac{T - T_{c,s}^0}{T_1 - T_{c,s}^0}. \quad (44)$$

This leads to the relation between the supercooling temperature $T_{c,s}^0$, the freezing point temperature T_c and the superheating temperature T_1

$$T_1 = \frac{9}{8} T_c - \frac{1}{8} T_{c,s}^0. \quad (45)$$

In contrast to the supercooling of the water it is difficult to superheat an ice crystal. After a superheating

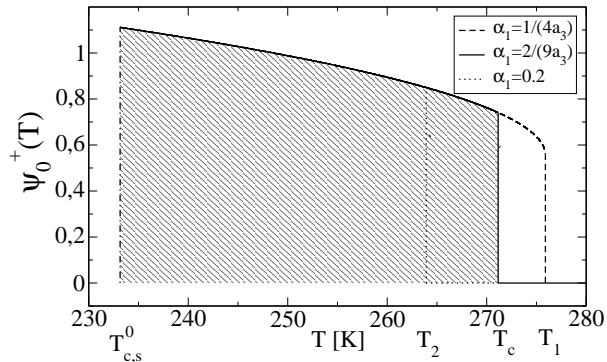


FIG. 8: Temperature-dependent representation of the supercooling region ($T < T_c$) and the superheating region ($T > T_c$).

of more than 5°C homogeneous nucleation occurs in the metastable state [34]. For fresh water ($T_c = T_0 = 273.15$ K and $T_{c,s}^0 = T_c^0 = 233.15$ K) if follows from equation (45) $T_1 = 278.11$ K (4.96°C) as the upper limit of superheating in agreement with the experiment [34].

Using (40) and (42) we can explain the values of α_1 and α_3 chosen for the numerical solution of the model equations in terms of water properties. We chose the structure parameter $\alpha_3 = 0.9$ such that for seawater of salinity 35 g/kg ($\rho_0 = 0.6$ mol NaCl/53 mol $\text{H}_2\text{O} = 0.0113$) the freezing point temperature is -1.9°C ($T_c = 271.25$ K). While dominated by Na^+ and Cl^- , seawater contains several other ions that influence its phase behaviour. Seawater is a multicomponent system that involves the crystallisation of some salts close to their respective eutectic concentrations. For temperatures $0 > T > -8^\circ\text{C}$, the influence of precipitating Ca^{2+} ions (in form of $\text{CaCO}_3 \cdot 6\text{H}_2\text{O}$) is almost negligible, but the onset of heavy precipitation of Na^+ ions (in form of mirabilite: $\text{Na}_2\text{SO}_4 \cdot 10\text{H}_2\text{O}$) below -8°C makes the theoretical description of the phase relationships in seawater more complicated. The precipitation of salt is not described by the presented model. Therefore, the model can be used to predict solidification structures only for the high temperature regime down to $\approx -8^\circ\text{C}$. The size of solidification structures depends on the supercooling relative to the freezing point T_c . The higher the supercooling, the more rapidly the water freezes and the smaller are the structures. Hence, discussing the time evolution of the salinity distribution and ice structure it is useful to perform the numerical simulation for high supercooling (but not below the precipitation temperature of mirabilite). Our choice of the freezing parameter $\alpha_1 = 0.2$ represents a temperature $T_2 = -8.2^\circ\text{C}$ in agreement with a frequently cited transition temperature of mirabilite. This along with (45) shows that with a structure parameter $\alpha_3 = 0.9$ and a freezing parameter $\alpha_1 = 0.2$ one has a realistic description of seawater at a temperature close to -8°C in terms of superheating and supercooling of pure water. For this case

the time evolution of the 2D patterns will be simulated with reasonable computing time using a small 128×128 grid. The morphology of the phase field structure as T approaches T_c is likely not altered, in particular because for $T_c > T > T_2$ a structural phase transition does not occur. However, the size of the structure ranges from μm to mm scale as discussed in the next section.

2. Diffusivity

The parameters α_1 and α_3 define the local portion of the free energy (15), which describes a system with uniform order parameter and salinity. The spatial inhomogeneity of the system is described by the third parameter of the model $D = D_{\text{ice}}/D_{\text{salt}}$. Spatial fluctuations of the order parameter are controlled by the diffusivity-type constant $D_{\text{ice}} = d_c^2/6\tau$, with the correlation length d_c and the relaxation time τ near the freezing point. We estimate the correlation length from the equilibrium radius $r_{i/w}$ of a spherical ice embryo formed from supercooled water near the freezing point. More recent theoretical simulations of ice nucleation involving the curvature effect on ice surface tension predict $r_{i/w} = 10^{-7}$ m (Fig. 5 in [35]). The classical nucleation theory has not been tested for ice crystal nucleation since there are no independent measurements of the ice surface tension. Instead, the validity of the theory has been assumed and the measured freezing point temperature has been used to obtain the value of the surface tension ([35] and ref. therein). The relaxation rate $1/\tau$ is proportional to reorientations of the H_2O -molecules per second, $1/\tau_d(T)$, which at the freezing point of fresh water assumes the value $1/\tau_d(T_0) = 0.5 \times 10^5 \text{ s}^{-1}$ [36]. With $d_c = 2 \times r_{i/w}$ and $\tau = \tau_d(T_0)$ it follows $D_{\text{ice}} = 0.33 \times 10^{-5} \text{ cm}^2/\text{s}$. The diffusion constant of salt D_{salt} we estimate from the counter-diffusion coefficient of the dominating salt in seawater NaCl

$$D_{\text{NaCl}} = \frac{(|Z_{\text{Na}^+}| + |Z_{\text{Cl}^-}|) D_{\text{Na}^+} D_{\text{Cl}^-}}{|Z_{\text{Na}^+}| D_{\text{Na}^+} + |Z_{\text{Cl}^-}| D_{\text{Cl}^-}}, \quad (46)$$

where D_{Na^+} and D_{Cl^-} are the tracer-diffusion coefficients of Na^+ and Cl^- , respectively. Z_{Na^+} and Z_{Cl^-} are the charges of the respective ions. Using the tracer-diffusion coefficients reported in [37] for 0°C at infinite dilution, $D_{\text{Na}^+} = 6.27 \times 10^{-6} \text{ cm}^2/\text{s}$ and $D_{\text{Cl}^-} = 10.1 \times 10^{-6} \text{ cm}^2/\text{s}$, it follows $D_{\text{NaCl}} = 0.77 \times 10^{-5} \text{ cm}^2/\text{s}$. Generally, the solute diffusion coefficient of aqueous solutions displays a weak salinity dependence. The diffusion coefficient in seawater is only about 8 per cent smaller than in water [37], i. e. $D_{\text{salt},0^\circ\text{C}} = 0.71 \times 10^{-5} \text{ cm}^2/\text{s}$. Most studies of aqueous NaCl have been restricted to temperatures above 0°C , and for D_{salt} only a few datasets extend down to 0°C . The required extrapolation to sub-zero temperatures can be found in [25]. At the freezing point temperature of seawater, -1.9°C , the study in [25] predicts $D_{\text{salt},-1.9^\circ\text{C}} = 0.62 \times 10^{-5} \text{ cm}^2/\text{s}$. The ratio

$D_{\text{ice}}/D_{\text{salt}} = 0.53$ obtained for the computed D_{salt} at -1.9°C may be compared to $D_{\text{ice}}/D_{\text{salt}} = 0.47$ based on the measured D_{salt} at 0°C . Hence we estimate for the model parameter $D = D_{\text{ice}}/D_{\text{salt}} = 0.5$.

B. Brine layer microstructures

As the two-dimensional interstitial liquid freezes, small ice bridges form between adjacent ice platelets, trapping inclusions of brine. Now that we have determined the three model parameters from the properties of water we can proceed and simulate the brine entrapment using our phase-field model. In figure 6 we show the time evolution of the salinity distribution and ice structure in the intercrystalline brine layer. We observe that structures found here are relative stable for a long time scale such that we assume them to be frozen. The final result of the structure is plotted in Fig. 9(d).

PRINGLE *et al.* [26] used sea ice single crystals, the building blocks of polycrystalline sea ice, to image their complex pore space with X-ray computed tomography. The structure of the brine pore space is seen in iso-surface plots in Fig. 9(a). The upper images clearly show near-parallel intracrystalline brine layers. However, the view across the layers (bottom images) show brine layer textures much more complicated than suggested by the simple model of parallel ice lamellae and parallel brine sheets illustrated in Fig. 9(b). Images at -18°C , -8°C and -4°C show a thermal evolution of the brine pore space where the porosity p changes from 2.2 to 4.6 to 8.8%. The connectivity increases with porosity as the pore space changes from isolated brine inclusions at $p = 2.2\%$ to extended, near-parallel layers at $p = 8.8\%$. PRINGLE *et al.* [26] characterized the thermal evolution of the brine pore space with percolation theory and demonstrated a connectivity threshold at a critical volume fraction $p_c = 4.6\%$. Below p_c there are no percolating pathways spanning a sample, i.e. the brine is trapped within the intracrystalline brine layers. In Fig. 9(c) we have chosen the best fit of the Turing-model [27] to the brine layer structure one observes very close to p_c . If we compare the simulation according to the here presented phase field model in Fig. 9 (d) the brine entrapment is better described by the short-time phase-field structures than by the Turing image.

Please note that the three parameters of the Turing model had been adjusted to fit the structure as best as possible. Here with the phase-field model we have chosen parameters according to the thermodynamic properties of water and have obtained the structure with these parameters. That the physical justification of the parameters by other properties of water leads here to a better description of the brine layer texture we consider as a demonstration of the importance of mass conservation invoked in the present model.

Now we are going to compare the size of the obtained structure with the size of pure sea ice platelets, separating

regions of concentrated seawater. Sea ice platelet spacing depends on the growth velocity of ice crystals in the basal plane [21], which is given as a function of salinity and supercooling ΔT_{sup} (relative to the freezing point T_c). The growth velocity of ice crystals is described by the empirical law $V = \gamma \times 1.87 \times 10^{-2} \Delta T_{\text{sup}}^{2.09}$, with V given in cm/s. Crystal growth in pure water is obtained for $\gamma = 1$ [39]. Ionic solutes do not considerably affect the growth kinetics, though the actual growth velocity at a given ΔT_{sup} will be changed by the factor γ . For NaCl solutions > 10 g/kg, γ falls monotonically with increasing solute concentration [40], a solution of 35 g/kg may decrease V by 50%. During phase separation, the water adjacent to the growing ice crystal becomes enriched in the rejected salt. The higher interfacial salt concentrations tend to depress the crystallization velocity more severely. The interface concentration is limited by the eutectic value of ≈ 230 g/kg. A NaCl solution of eutectic composition reduces the growth velocity by up to 86%. With $\gamma = 0.14$ and the chosen supercooling $\Delta T_{\text{sup}} = T_c - T_2 = 6.3$ K we obtain $V = \gamma \times 1.87 \times 10^{-2} \Delta T_{\text{sup}}^{2.09} = 1.2 \times 10^{-1}$ cm/s. Using the result for V , the size of sea ice platelets can be obtained from the morphological stability theory. For $V \approx 0.1$ cm/s, the morphological stability analysis predicts a wave length of most rapidly growing perturbations of $\lambda_{\text{max}} \approx 1 \mu\text{m}$ (see Fig. 2 in [21]).

Now we use equation (38) to calculate the critical domain size of the phase field structure as a function of the freezing point depression. The critical domain size is determined by the fastest-growing wave-vector κ_c (33). From the relation between the dimensionless wavenumber κ , the dimensional wavenumber k and equation (38) we get the minimum size of the structure

$$\lambda_c = \frac{2\pi}{k_c} = \frac{2\pi}{\kappa_c} \sqrt{\frac{M}{\Gamma}} \frac{h}{a_2} = \frac{2\pi}{\kappa_c} \sqrt{\frac{D_{\text{salt}} \rho_0}{\Gamma \tilde{a}_1 |\Delta T|}}, \quad (47)$$

with $2\pi/\kappa_c = 13.81$ and the parameters specified in the previous section: $D_{\text{salt}} = 0.71 \times 10^{-5}$ cm²/s, $\rho_0 = 0.0113$, and $|\Delta T| = 1.9$. The parameter left to be determined is $\Gamma \tilde{a}_1$. This parameter we derive from the temperature dependence of the order parameter kinetics (4), which is described by the rate constant $\Gamma a'_1 = \Gamma a'_1(T)$ for the change of the dimensional order parameter u . The rate $\Gamma a'_1(T)$ is proportional to reorientations of the H₂O-molecules per second, $1/\tau_d(T)$, which at the freezing point of fresh water, $T_0 = 273.15$ K, assumes the value $1/\tau_d(T_0) = 0.5 \times 10^5$ s⁻¹ [36]. Because of the requirement that $a'_1(T_c^0) = 0$ at the lower limit of the supercooling region, $T_c^0 = 233.15$ K, the rate $\Gamma a'_1(T)$ is approximated by

$$\Gamma a'_1(T) = \Gamma \tilde{a}_1 (T - T_c^0) \sim \frac{1}{\tau_d(T)}. \quad (48)$$

The temperature-independent coefficient $\Gamma \tilde{a}_1$ we estimate from $\Gamma a'_1(T_0) = \frac{1}{\tau_d(T_0)}$, i. e. we assume $\Gamma \tilde{a}_1 = 1/[(T_0 - T_c^0)\tau_d(T_0)] = 1250$ K⁻¹ s⁻¹. Our choice of the

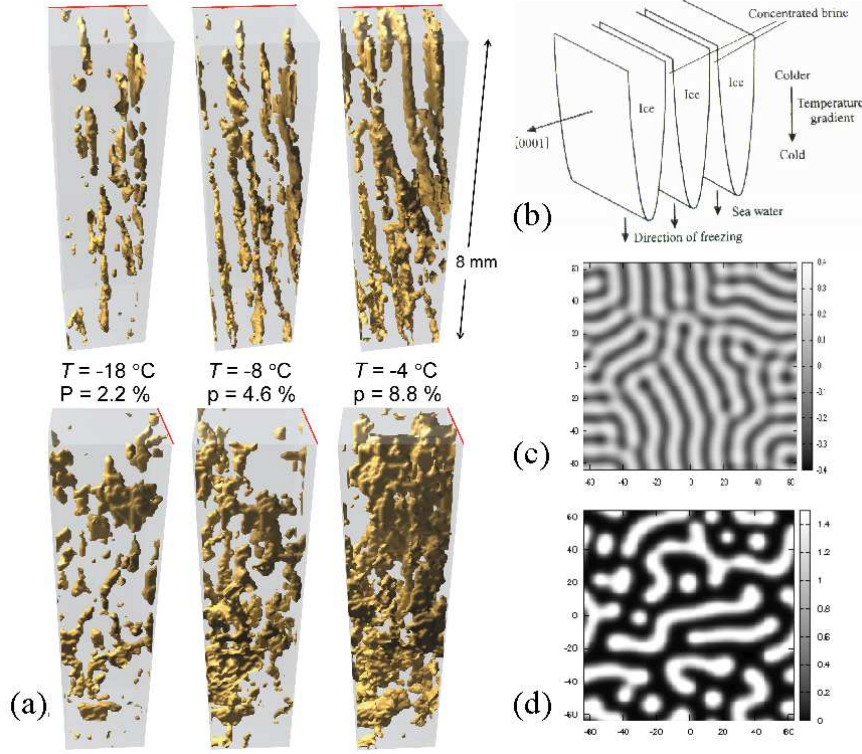


FIG. 9: (a) Imaging brine pore space with X-ray computed tomography (image from [26]). The upper images shows the view approximately along the brine layers. The view across the brine layers (of the same volumes rotated about the vertical axis by 90°) is shown in the bottom images. (b) Sea ice crystal composed of parallel plates of pure ice with concentrated brine in layers between them (image from [38]). (c) Turing structure for $\tau = 400$ [27], (d) phase field structure for $\tau = 500$ from figure 6.

freezing parameter $\alpha_1 = 0.2$ represents a supercooling $\Delta T_{sup} = 6.3$ K. For this growth condition we obtain from equation (47) a critical domain size $\lambda_c = 0.8 \mu\text{m}$ in agreement with the sea ice platelet spacing $\lambda_{max} \approx 1 \mu\text{m}$ obtained from morphological stability analysis [21]. Please note that our choice of 6.3 K supercooling does not represent the natural conditions observed in the oceans. Supercoolings are commonly believed to be small (< 0.1 K) owing to the abundant presence of impurities upon which nucleation of ice crystals occurs via heterogeneous mechanisms [41]. Heterogeneous nucleation processes are responsible for virtually all of the ice on earth.

In nature, fresh water is never totally pure. While supercooling in pure water has been observed down to -40°C , the presence of small impurities commonly initiate freezing at temperatures between -15°C and -20°C [42]. The observed sea ice plate spacings are 2 – 3 orders of magnitude larger than $1 \mu\text{m}$. The thickness of ice lamellae between brine layers reported in [26] was in the range of 200-500 μm (see Fig 1a). Brine inclusions described by WEISSENBARGER [43] had scales from below 3 to 1000 μm , where the average dimensions were typically 200 μm . The size of the phase-field structures for natural conditions are described by the upper limit of the instability region shown in Fig. 4. With a structure parameter $\alpha_3 = 1.99$ and a freezing parameter $\alpha_1 = 0.111482$ one

has a realistic description of seawater at 0.032 K supercooling and a lower limit of the supercooling region of fresh water at -18.78°C . For this growth condition we obtain from equation (33) the dimensionless structure size $2\pi/\kappa_c = 4975.25$. Using equation (47) we obtain a critical domain size $\lambda_c = 198 \mu\text{m}$ in agreement with the observed values.

V. CONCLUSION

A phase field model for brine entrapment in sea ice is developed which describes the time evolution of the micro-scale inclusions in the absence of spatial temperature gradients in ice or water. The coupled evolution equations are derived from a generating functional in such a way that the mass conservation law for salt is preserved. The resulting equations are different from the earlier used Turing model which does not include conservation of salt. Though the same number of three parameters are used the phase field model allows to determine them by physical properties and lead to a better agreement with experimental brine layer textures.

The linear stability analysis provides the phase diagram in terms of two parameters indicating the region where spatial structures can be formed due to the insta-

bility of the uniform ordered phase. The region of instability is determined exclusively by the freezing parameter and the structure parameter and not by the diffusivity as it was the case in the Turing model. This allows to link the freezing and structure parameter to thermodynamic properties of water like superheating, supercooling and freezing temperature.

With the help of the parameters determined by the properties of water we solve the time-dependent coupled evolution equations and determine the micro-scale brine network. Since, the brine tends to be located in vertically oriented sheet-like inclusions, we performed the numerical simulations in two dimensions. A good agreement with the experimental brine layer texture is achieved. Therefore we believe that the simulation of the short-time frozen microstructures led to a realistic description

of the early phase of brine entrapment. Brine inclusions that evolve in the long-term show length scales from sub-millimeter brine layers to meter long brine channels. The description of the brine channel formation requires simulations on large scales in three-dimensional domains including a detailed description of the thermal evolution of brine inclusions. The quite demanding large scale simulations will be the subject of future research.

Acknowledgments

This work was supported by DFG-priority program SFB 1158. The financial support by the Brazilian Ministry of Science and Technology is acknowledged.

-
- [1] K. R. Arrigo, D. L. Worthen, M. P. Lizotte, P. Dixon, and G. Dieckmann, *Science* **276**, 394 (1997).
- [2] G. S. Dieckmann and H. H. Hellmer, in *Sea Ice*, edited by D. N. Thomas and G. S. Dieckmann (John Wiley & Sons, Chichester, 2010), chap. 1.
- [3] W. F. Weeks and S. F. Ackley, in *The Geophysics of Sea Ice*, edited by N. Untersteiner (Plenum Pr., New York, 1986), pp. 9–164.
- [4] H. Eicken, in *Sea Ice: an introduction to its physics, chemistry, biology and geology*, edited by D. N. Thomas and G. S. Dieckmann (Blackwell Science Ltd, Oxford, 2003), chap. 2.
- [5] K. R. Arrigo, D. H. Robinson, and C. W. Sullivan, *Mar. Ecol. Prog. Ser.* **98**, 173 (1993).
- [6] P. M. Lizotte, *American Zoologist* **41**, 57 (2001).
- [7] D. N. Thomas and G. S. Dieckmann, *Science* **295**, 641 (2002).
- [8] G. Quincke, *Proceedings of the Royal Society of London* **76**, 431 (1905).
- [9] W. A. Tiller, K. A. Jackson, J. W. Rutter, and B. Chalmers, *Acta Metallurgica* **1**, 428 (1953).
- [10] B. Chalmers, *Principles of Solidification* (John Wiley & Sons, New York, 1964).
- [11] M. G. Worster and J. S. Wettlaufer, *J. Phys. Chem. B* **101**, 6132 (1997).
- [12] D. L. Feltham, N. Untersteiner, J. S. Wettlaufer, and M. G. Worster, *Geophysical Research Letters* **33** (2006).
- [13] K. M. Golden, S. F. Ackley, and V.I.Lytle, *Science* **282**, 2238 (1998).
- [14] K. M. Golden, A. L. Heaton, H. Eicken, and V. I. Lytle, *Mechanics of Materials* **38**, 801 (2006).
- [15] K. M. Golden, H. Eicken, A. L. Heaton, J. Miner, D. J. Pringle, and J. Zhu, *Geophysical Research Letters* **34**, 16501 (2007).
- [16] S. F. Ackley and C. W. Sullivan, *Deep-Sea Research I* **41**, 1583 (1994).
- [17] I. Werner, J. Ikävalko, and H. Schünemann, *Polar Biology* **30**, 1493 (2007).
- [18] W. A. Tiller, in *The art of science of growing crystals*, edited by J. J. Gilman (John Wiley & Sons Inc, New York, 1963), chap. 15.
- [19] W. W. Mullins and R. F. Sekerka, *Journal of Applied Physics* **35**, 444 (1964).
- [20] S. R. Coriell, G. B. McFadden, and R. F. Sekerka, *Ann. Rev. Mater. Sci.* **15**, 119 (1985).
- [21] J. S. Wettlaufer, *Europhys. Lett.* **19**, 337 (1992).
- [22] A. Tiller, *The Science of Crystallization: Microscopic Interfacial Phenomena* (Cambridge University Press, Cambridge (England), 1991).
- [23] A. Tiller, *The Science of Crystallization: Macroscopic Phenomena and Defect Generation* (Cambridge University Press, Cambridge (England), 1991).
- [24] D. T. J. Hurle, *Handbook of Crystal Growth*, vol. 1+2 (Elsevier Science Ltd, Amsterdam, 1993).
- [25] S. Maus, *On Brine Entrapment in Sea Ice: Morphological Stability, Microstructure and Convection* (Logos, Berlin, 2007).
- [26] D. J. Pringle, J. E. Miner, H. Eicken, and K. M. Golden, *Journal of Geophysical Research* **114** (2009).
- [27] B. Kutschan, K. Morawetz, and S. Gemming, *Phys. Rev. E* **81**, 036106 (2010).
- [28] D. Grandi, *Z. Angew. Math. Phys.* **64**, 1611 (2013).
- [29] N. N. Medvedev and Y. I. Naberukhin, *J. Non-Cryst. Solids* **94**, 402 (1987).
- [30] W. C. Röntgen, *Ann. Phys. (Leipzig)* **45**, 91 (1892).
- [31] S. M. Cox and P. C. Matthews, *Journal of Computational Physics* **176**, 430 (2002).
- [32] A. N. Nevzorov, *Izvestiya, Atmospheric and Oceanic Physics* **42**, 765 (2006).
- [33] N. E. Dorsey, *Properties of ordinary water-substance* (Reinhold Publishing Corp., New York, 1940).
- [34] K. Baumann, J. H. Bigram, and W. Känzig, *Z. Phys. B - Condensed Matter* **56**, 315 (1984).
- [35] A. Bogdan, *J. Chem. Phys.* **106**, 1921 (1997).
- [36] D. Eisenberg and W. Kauzmann, *The structure and properties of water* (Clarendon Press, Oxford, 2005).
- [37] Y.-H. Li and S. Gregory, *Geochim. Cosmochim. Acta* **38**, 703 (1974).
- [38] V. F. Petrenko and R. W. Whitworth, *Physics of Ice* (Oxford University Press, Oxford, New York, 1999).
- [39] S. H. Tirmizi and W. N. Gill, *Journal of Crystal Growth* **85**, 488 (1987).
- [40] J. G. Vlahakis and A. J. Barduhn, *AIChE Journal* **20**, 581 (1974).

- [41] C. Petrich and H. Eicken, in *Sea Ice*, edited by D. N. Thomas and G. S. Dieckmann (John Wiley & Sons, Chichester, 2010), chap. 2.
- [42] D. E. Hagen, R. J. Anderson, and J. L. Kassner, *J. Atmos. Sci.* **38**, 12361243 (1981).
- [43] J. Weissenberger, *Ber. Polarforschung* **111**, 1 (1992).